Single-crystal diffraction at the Extreme Conditions beamline P02.2: procedure for collecting and analyzing high-pressure single-crystal data

André Rothkirch,[a]* G. Diego Gatta,[b] Mathias Meyer,[c] Sébastien Merkel,[d] Marco Merlini[b] and Hanns-Peter Liermann[a]

[a]Deutsches Elektronen Synchrotron DESY, Hamburg, Germany, [b]Dipartimento Scienze della Terra, Università degli Studi di Milano, Via Botticelli 23, I-20133 Milano, Italy, [c]Agilent Technologies (Poland) Sp. z o.o., ul. Szarskiego 3, PL-54-609 Wroclaw, Poland, and [d]Unité Matériaux et Transformations, ENSCL, CNRS, Université Lille 1, 59655 Villeneuve d'Ascq, France.
E-mail: andre.rothkirch@desy.de

Fast detectors employed at third-generation synchrotrons have reduced collection times significantly and require the optimization of commercial as well as customized software packages for data reduction and analysis. In this paper a procedure to collect, process and analyze single-crystal data sets collected at high pressure at the Extreme Conditions beamline (P02.2) at PETRA III, DESY, is presented. A new data image format called 'Esperanto' is introduced that is supported by the commercial software package *CrysAlis*^{Pro} (Agilent Technologies UK Ltd). The new format acts as a vehicle to transform the most common area-detector data formats *via* a translator software. Such a conversion tool has been developed and converts tiff data collected on a Perkin Elmer detector, as well as data collected on a MAR345/555, to be imported into the *CrysAlis*^{Pro} software. In order to demonstrate the validity of the new approach, a complete structure refinement of boron-mullite (Al_5BO_9) collected at a pressure of 19.4 (2) GPa is presented. Details pertaining to the data collections and refinements of B-mullite are presented.

Keywords: Extreme Conditions beamline (P02.2); PETRA III; high-pressure single-crystal diffraction; data collection; data reduction; Esperanto data format.

1. Introduction

Single-crystal diffraction in the diamond anvil cell (DAC) is a widely used technique to determine the full structural behavior of condensed matter on an atomistic level as a function of high pressure at room temperature. For many years this technique has been employed mainly at laboratory X-ray sources equipped with four-circle diffractometers using point detectors and more recently CCDs (Angel *et al.*, 2000). Because of the large size of the X-ray beam originating from the X-ray tube or rotating anode, many of these experiments have been limited to pressures below 12 GPa at which the preferred pressure medium of methanol:ethanol:H_2O (16:3:1) freezes (Angel *et al.*, 2007). Using compressed gases of Ne or He as a pressure-transmitting medium and very small crystals have pushed the quasi-hydrostatic pressure limit significantly higher (Klotz *et al.*, 2009) so that a maximum pressure is not yet in sight (Jacobsen *et al.*, 2008). Thus, today the limiting factor for conducting single-crystal diffraction is the brilliance of the laboratory-based sources that make it impossible to collect adequate data at higher pressures when

the single crystals are very small. For this reason, many higher-pressure experiments are conducted at third-generation light sources. There has been a push in the last decade to establish single-crystal experiments for full structure analysis in the DAC at beamlines optimized for high-pressure diffraction (Dera *et al.*, 2005, 2008, 2011a,b; Jacobsen *et al.*, 2008; Plonka *et al.*, 2012; Zhang *et al.*, 2012; Lavina *et al.*, 2010a,b; McMahon *et al.*, 2003, 2007a,b; Lundegaard *et al.*, 2009; Maynard-Casely *et al.*, 2010; Marques *et al.*, 2011; Guillaume *et al.*, 2011; Chaimayo *et al.*, 2012). In the early stages, this development of adequate software to collect, reduce and analyze single-crystal data sets was limited to the use of 'slower' area detectors (MAR345 IP or MAR165 CCD), but in the past five years the use of the MAR555 fast flat-panel detector at, for example, beamline ID9 at the ESRF has reduced collection times significantly (Merlini *et al.*, 2012a,b; Kantor *et al.*, 2012).

Nevertheless, the ever increasing brilliance of the third-generation light sources and the superior performance of new detectors (*e.g.* Pilatus detectors, Perkin Elmer XRD1621 *etc.*) particularly at higher energies require the optimization of commercial as well as customized software packages, to make

optimal use of beam time at the third-generation light sources. In fact, such new generation flat-panel detectors allow the data collection of full single-crystal datasets on the timescale of a few minutes and detailed structural investigation of crystals at very high pressures and temperatures (Dubrovinsky *et al.*, 2010; Boffa Ballaran *et al.*, 2012; Merlini *et al.*, 2012*b*).

Within this paper we describe the data collection and data reduction procedure developed for the Extreme Conditions beamline (ECB P02.2) at PETRA III, DESY, Hamburg, Germany. This includes the introduction of a new data format called 'Esperanto' that is supported by the commercial software package *CrysAlis*^{Pro} (Agilent, 2013) and that provides a vehicle to transform the most common area-detector data formats employed at high-pressure beamlines using appropriate translator software. In order to illustrate the performance of the new set-up and data treatment procedure, we also show and analyze single-crystal data collected in the DAC at high pressure and room temperature. These data provide first impressions of the performance of the fast flat-panel detector XRD1621 from Perkin Elmer for conducting single-crystal diffraction experiments.

2. Goniometer set-up and data collection procedure at the ECB for single-crystal diffraction

2.1. Goniometer set-up

Single-crystal diffraction at the ECB can be performed on the basis of single horizontal rotation (ω) with a maximum range of $\pm 45°$ (only $+30°$ on the general-purpose experiment) with a detector in forward geometry. Rotation in χ, φ and 2θ, commonly available at crystallographic beamlines or laboratory-based four-circle diffractometers, are not absolutely necessary when conducting single-crystal diffraction at high pressure in the DAC, because of the limited access to reciprocal space. Alignment of the sample in the DAC is accomplished by placing the sample into the rotation center of the ω rotation. For this purpose, the sample positioning stack offers two horizontal translations (along and parallel to the beam) above and below the ω rotation. The lower translations ensure positioning of the center of the ω rotation into the beam, whereas the upper translations enable positioning of the sample into the ω rotation center. This set-up provides a sphere of confusion of about 1 μm within the maximal range of rotation. Alignment of the detector with respect to the ω rotation center is not necessary because the detector is located in transmission geometry perpendicular to the incident X-ray beam. Rough positioning with respect to orthogonal alignment may be accomplished by tilting and rotating the detector positioning and cross checking the final position within, for example, *fit2d* (Hammersley *et al.*, 1996). Alternatively, one may use step scans from a ruby sphere from NIST (Wong-Ng *et al.*, 2001) to calibrate the sample-to-detector distance as well as non-orthogonal alignment within *CrysAlis*^{Pro}. In addition, the detectors may be positioned on a virtual Ewald's sphere using the horizontal rotation underneath the detector and the two horizontal translations parallel and perpendicular to the
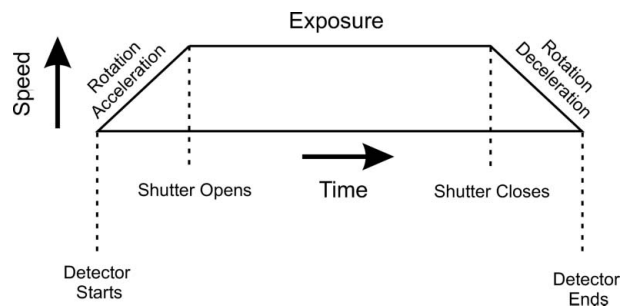
Figure 1
Schematic view of the data collection approach employed.

beam. The latter is currently limited to a maximum of $\pm 25°$ rotations.

2.2. Data collection procedure using the MAR345 and the Perkin Elmer detector

At the ECB, single-crystal diffraction data are collected by simple ω scans following the data collection procedure employed by *CrysAlis*^{Pro} on their commercial diffractometer. Diffraction data were collected in step scans as illustrated in Fig. 1.

After centering the DAC on the beamline sample stack, we use an in-house script that was written in Python and interacts with the online control system (Tango) (Alfaro *et al.*, 2011). The script requires the following input information: `<file name>` `<start omega>` `<end omega>` `<step size>` `<time per step>`.

From this information the script calculates the ω start and end angle taking into account the acceleration and deceleration of the ω stepping motor in order to reach a constant speed when the rotation reaches the scan starting angle. The exposure of the detectors is timed such that the script checks every 10 ms during the acceleration whether the scan position has been reached and opens the internal shutter of the beamline to expose the detector up on arrival. During the exposure, the scripts continually check whether the end position of the scan has been reached and closes the shutter after arrival and decelerates the stepper motor. For all consecutive scans, the above procedure is repeated until all step scans are completed. All essential parameters of the scan are collected and stored in a separate file, *i.e.* motor position of the sample stack especially the ω rotation (start and end scan) and ion chamber readings before the focusing device. Readout of the diffraction images taken during the step scan on the respective area detector proceeds as follows depending on the detector.

2.2.1. MAR345. In the case of the MAR345, a Tango server receives a message from the script to execute a scan using the mar345dtb program of the image plate after the shutter is closed. The script waits until the scan is completed and continues with the next step scan. In such an operation mode, no metadata (*e.g.* angular positions) are embedded into the header of the MAR image data. This has to be added in a separate processing step after the experiment if needed (see Appendix C).

2.2.2. Perkin Elmer XRD 1621. For the XRD 1621 flat-panel detector from Perkin Elmer, a more evolved collection procedure has been developed. In order to control the XRD 1621, we use the windows-based software *QXRD* developed as freeware by G. Jennings (Jennings, 1997). This program controls the XRD 1621 and allows, beside others, long exposures to be taken *via* the summation of multiple exposures (0.067 s to 8 s for a single contributing exposure) including the subtraction of the dark current for each image. The summation of multiple images to one image is necessary because beyond 8 s the XRD 1621 has an inherently large dark current that can overcome the actual diffraction signal. The relative small dynamic range of the detector can cause considerable problems when the detector is being over-saturated, especially by the single-crystal spots originating from the diamond anvil. In order to overcome the above limitation of the XRD 1621, the script 3D-XRD-HR collects a dark image at the beginning of a step-scan series. Ideally, the detector should have been idle for a while giving it the opportunity to eliminate afterglow through continuous readout prior to the start of the experiment. The script calculates the exposure time in increments of 1 s if the exposure time is longer than 1 s, *i.e.* it divides an n s exposure into $n \times 1$ s exposures that are combined into one image at the end of the exposure. Each 1 s image is corrected by the dark image before summation. Exposures lasting less than 1 s are collected at their respective exposure times. However, because the Perkin Elmer detector is refreshed every 0.067 s, synchronizing the detector with the opening of the shutter and the start of the exposure is rather difficult. Thus, the script starts the detector when it starts the step scan during the acceleration of the stepper motor. In this way the detector is already accumulating images when the shutter is being opened through the script avoiding any delays due to the timing delay of the detector. Of course, the overall exposure has to be longer than the actual exposure, *i.e.* we programmed the script to collect diffraction images during the entire rotation including acceleration and deceleration. After each exposure, the script waits until the detector has finished saving the image, which takes usually less than 0.1 s. Finally, we have implemented a delay loop to counteract any oversaturation and afterglow that could be problematic during the analysis of very strong reflections. For this reason, we read out the detector ten times at its minimum exposure time of 0.067 s dictated by the readout speed of the detector. The images are displayed in *QXRD* and work as a control mechanism for overexposures. These 'clearing' images are deleted before each new step scan.

2.3. Data preparation and parameter setting for reduction with *CrysAlis*^{Pro}

In order to prepare MAR345 (Marresearch GmbH) as well as Perkin Elmer (PerkinElmer Inc.) image data for further analysis with the software package *CrysAlis*^{Pro}, we developed a converter tool. The tool is written in IDL (Interactive Data Language, by Exelis Visual Information Solutions) and

provides input options for defining experiment-specific parameters inside the image data for interpretation by *CrysAlis*^{Pro}. If the image data were recorded by a MAR345/555 detector, the tool only modifies image header data and preserves the usually compressed binary section of the data. In the case where data were collected by, for example, a Perkin Elmer detector, the tool converts image data into the newly invented *CrysAlis*^{Pro} Esperanto format that is supported in *CrysAlis*^{Pro} (version 1.171.36.28 or higher). In both cases the tool modifies the values of the φ angle inside the header of each image of a series. Note that the pure ω scan at the beamline (equipped with one circle only) is interpreted in *CrysAlis*^{Pro} as a φ scan. To do so, the first and last file of an image series needs to be selected as well as an output directory, starting value for the φ angle and a step width 'Delta PHI' of the step scan. In addition, the tool makes it possible to select the scan direction and detector mounting by setting the flags 'counter-clockwise rotation', 'transpose data' or 'flip vertical', respectively. A screenshot of the user interface is given in Fig. 2. Currently, the tool can convert image formats of the MAR345 as well as tiff images, *e.g.* from the Perkin Elmer detector XRD1621 created *via QXRD* (Jennings, 1997). The 'Advanced Opt.' button offers different settings for modifying the header information. See Appendix C for further details.

The converted (or prepared) detector images are successively analyzed with the *CrysAlis*^{Pro} software (version 1.171.36.28), which benefits from a number of options suitable for high-pressure work, including the determination of the DAC opening cone shadow as a function of ω angles, algo-
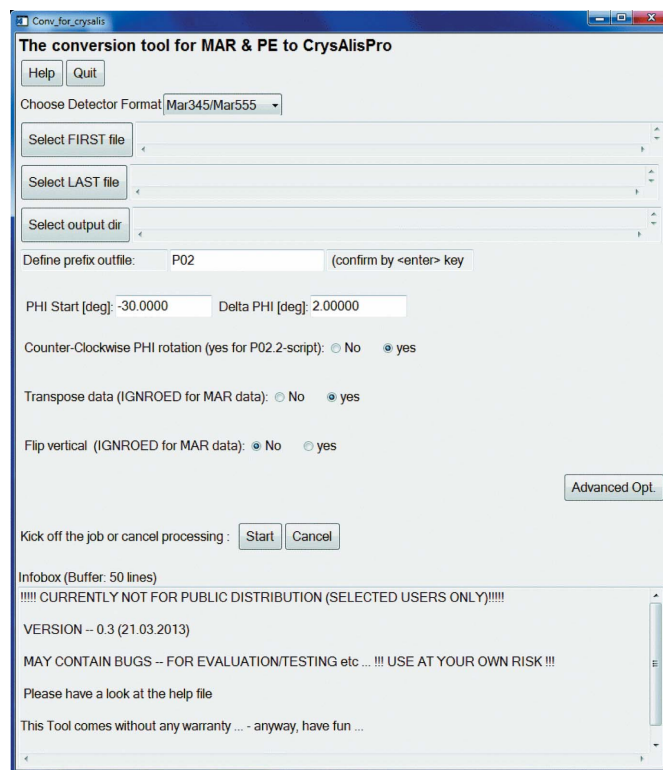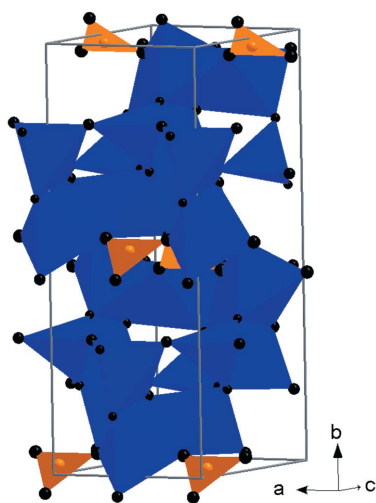

Figure 2
Graphical user interface (Toplevel GUI) of the conversion tool at P02.2, DESY, *i.e.* to provide scan ranges applied in an experiment.

rithms for detection and rejection of outliers, and Friedel's pair or symmetry-based rescaling algorithms.

3. Test experiment at high pressure: the case of B-mullite

Test experiments have been performed in order to describe the elastic behavior and the pressure-induced structure evolution of Al_5BO_9 (hereafter 'B-mullite'), a ceramic material, at pressures in excess of 7 GPa.

The crystal structure of this compound was solved and refined by Sokolova *et al.* (1978) in the space group $Cmc2_1$ [a = 5.6673 (7), b = 15.011 (2), c = 7.693 (1) Å], and recently re-investigated by Gatta *et al.* (2010). Its structure consists of mullite-type octahedral chains, linked by edge-sharing AlO_5 bipyramids alternating with AlO_4 tetrahedra and BO_3 triangular units (Fig. 3). Gatta *et al.* (2010) investigated the elastic behavior and the pressure-induced structure evolution of Al_5BO_9 by *in situ* single-crystal X-ray diffraction up to 7 GPa with a DAC and under hydrostatic conditions, in the home laboratory. No phase transition or anomalous compressional behavior occurred within the investigated pressure (P) range. Fitting the pressure–volume (P–V) data with a truncated second-order (in energy) Birch–Murnaghan equation of state (BM-EoS), using the data weighted by the uncertainties in P and V, they obtained V_0 = 656.4 (3) Å^3 and K_{T0} = 165 (7) GPa [β_{V0} = 0.0061 (3) GPa^{-1}]. Axial compressibility coefficients yielded: β_a = 1.4 (2) × 10^{-3} GPa^{-1}, β_b = 3.4 (4) × 10^{-3} GPa^{-1} and β_c = 1.7 (3) × 10^{-3} GPa^{-1} ($\beta_a : \beta_b : \beta_c$ = 1:2.43:1.21). The structure refinement at high pressure allowed the description of the main deformation mechanisms at the atomic scale. However, the drastically low compressibility of this compound hindered an exhaustive description of the elastic behavior and the pressure-induced structure rearrangement, suggesting that only a new experiment at pressures in excess of 7 GPa would

allow the open questions about the pressure behavior of Al_5BO_9 to be answered. In this light, B-mullite was selected as a good candidate for a test experiment at a pressure in excess of 7 GPa.

High-pressure synchrotron single-crystal diffraction data up to 25.6 (2) GPa were collected at beamline P02.2 using X-rays with 0.28988 Å wavelength and a focusing spot of ∼8.5 μm (H) × 1.8 μm (V), originating from a compound refractive lens system consisting of 121 Be lenses with a radius of 50 μm (400 μm beam acceptance) and a focal length of 1221 mm. A platey single crystal of B-mullite (∼40 μm × 40 μm × 5 μm) was loaded in a symmetric DAC, equipped with Boehler Almax design diamonds/seats with a 70° opening and 300 μm culets size. A 250 μm-thick rhenium gasket was pre-indented to 60 μm and then drilled with a 200 μm hole, in which the crystal of B-mullite, along with some calibrated ruby spheres for pressure determination (Mao *et al.*, 1986), were located. Neon was used as the hydrostatic pressure-transmitting medium (Klotz *et al.*, 2009). Pressure was increased with an automated pressure-driven system and measured with the online ruby/alignment system. Diffraction images were acquired on a Perkin Elmer XRD 1621 flat-panel detector, using the in-house script previously described for collecting step-scan diffraction images. The sample-to-detector distance (402.34 mm) was calibrated using a CeO_2 standard (NIST 674a). The images were then converted to the Esperanto format, as previously described, in order to be readable by the program *CrysAlis^{Pro}*. A pure ω-scan ($-30°$ ≤ ω ≤ $+30°$), with a step size of 1° and an exposure time of 2 s per frame was used. Bragg peaks were then indexed and their intensities were integrated and corrected for Lorentz-polarization effects, using the *CrysAlis^{Pro}* package. The reflection conditions were consistent with those of the space group $Cmc2_1$ within the entire P-range investigated. High-P structure refinements have successfully been performed up to the maximum pressure. As an example, we report in Table 1 the data pertaining to the structure refinement of B-mullite at 19.4 (2) GPa, the refined atomic positions and their isotropic displacement parameters (see CIF[1] for additional details). The un-warped single-crystal diffraction patterns (based on raw data) of the ($hk2$)* plane, in which the lattice is clearly C-centered, and the graphical output of *CrysAlis^{Pro}* with a section of the Ewald sphere are shown in Fig. 4.

This synchrotron experiment showed that Al_5BO_9 preserves its crystallinity in the crystal structure first described by Gatta *et al.* (2010), at least up to 25–26 GPa. Al_5BO_9 displays a significant stiffness. Its isothermal bulk modulus, obtained in this study by a second-order BM-EoS fit, is 164 (1) GPa. This value is in good agreement with the experimental findings of Gatta *et al.* (2010) [*i.e.* 165 (7) GPa], based on data collected up to about 7 GPa. The limited P-range investigated by Gatta *et al.* (2010) hindered a thorough description of the main mechanisms, at the atomic scale, in response to the applied

Figure 3
Clinographic of the crystal structure of B-mullite based on the structure refinement at 19.4 (2) GPa. Al polyhedra are shown in dark grey (blue online), B triangles in light grey (orange online).

---

[1] Supplementary data for this paper are available from the IUCr electronic archives (Reference: FV5010). Services for accessing these data are described at the back of the journal.

Table 1
Details pertaining to the data collections and refinements of B-mullite at 19.4 (2) GPa.

P (GPa)	19.4 (2)
X-ray radiation (Å)	0.28988
Reference formula	Al_5BO_9
Z	4
Data collection method	ω scans, 1° frame^{-1}, 2 s frame^{-1}
Space group	$Cmc2_1$
a (Å)	5.549 (2)
b (Å)	14.350 (6)
c (Å)	7.481 (2)
Maximum 2θ (°)	24.44
Measured reflections	449
Unique reflections	341
Unique reflections with $I > 3\sigma(I)$	223
R_{int}	0.051
No. of refined parameters	30
$R_1, I > 3\sigma(I)$	0.0581
wR_2	0.0891
Residuals (e Å^{-3})	+0.9/−0.8

Site	x	y	z	U_{iso}
Al1 (8b)	0.2510 (6)	0.1172 (4)	0.33664	0.0111 (6)
Al2 (4a)	0	0.2560 (5)	0.5196 (11)	0.0111 (6)
Al3 (4a)	0	0.4454 (5)	0.5296 (13)	0.0111 (6)
Al4 (4a)	0	0.3018 (6)	0.1671 (12)	0.0111 (6)
B (4a)	0	0.0167 (19)	0.060 (2)	0.012 (5)
O1 (4a)	0	0.3241 (14)	0.710 (2)	0.0161 (11)
O2 (8b)	0.2528 (15)	0.1877 (9)	0.5402 (17)	0.0161 (11)
O3 (4a)	0	0.4528 (12)	0.909 (2)	0.0161 (11)
O4 (4a)	0	0.0424 (12)	0.417 (2)	0.0161 (11)
O5 (4a)	0	0.3544 (15)	0.369 (2)	0.0161 (11)
O6 (4a)	0	0.1925 (15)	0.262 (2)	0.0161 (11)
O7 (8b)	0.2141 (14)	0.0472 (9)	0.1317 (18)	0.0161 (11)

Note: $R_{int} = \sum |F_{obs}^2 - \bar{F}_{obs}^2| / \sum (F_{obs}^2)$; $R_1 = \sum (|F_{obs}| - |F_{calc}|) / \sum |F_{obs}|$; $wR_2 = \{\sum [w(F_{obs}^2 - F_{calc}^2)^2] / \sum [w(F_{obs}^2)^2]\}^{1/2}$, $w = 1/[\sigma^2 F_{obs}^2 + (0.01P)^2]$, $P = [\max(F_{obs}^2, 0) + 2F_{calc}^2]/3$. Isotropic displacement parameters refined by grouping all of the Al sites and all of the O sites. Structure refinement performed with *Jana2006* (Petricek *et al.*, 2006).

pressure, because up to 7 GPa all the building block units of the structure (*i.e.* Al-polyhedra, BO_3-unit) behave as rigid units. The higher P-range investigated in this study allowed a description of the compressional behavior of the chemical bonds, along with the intra-polyhedral deformation coupled with noticeable inter-polyhedral tilting. The chains of edge-sharing octahedra run along [100] in Al_5BO_9. Such chains act as 'pillars': the deformation along the chain direction is controlled by compression of the octahedral bonds; poly-hedral tilting cannot occur along the chain direction in order to accommodate the deformation energy. On the contrary, the presence of pentagonal voids on the plane perpendicular to the octahedral chains [*i.e.* (100)] allows the strain energy to be accommodated by polyhedral tilting, making the structure of Al_5BO_9 more compressible on this plane. Further details pertaining to experimental protocols, data reduction, structure refinements, elastic behavior and P-induced deformation mechanisms in Al_5BO_9 up to 26 GPa will be provided by Gatta *et al.* (2013).

4. Summary

Single-crystal diffraction experiments in the diamond anvil cell are now standard at third-generation light sources, in
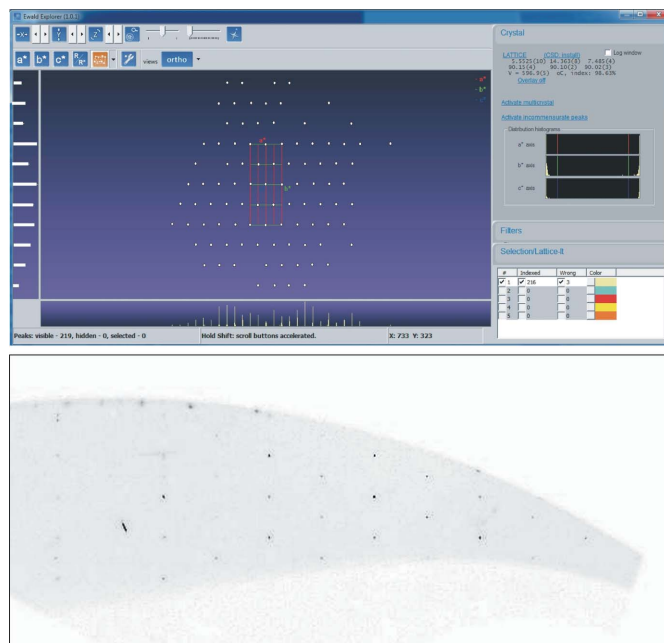
Figure 4
Top: graphical output of *CrysAlis*^{Pro} (using the tool EwaldPro) with a section of the Ewald sphere of B-mullite at 19.4 (2) GPa. Bottom: un-warped single-crystal diffraction patterns (based on raw data) of the $(hk2)*$ plane, in which the C-centered lattice is clear.

particular at beamlines optimized for high-pressure diffraction. Within recent years, new detectors have significantly reduced collection times and require the optimization of commercial as well as customized software packages to make optimal use of beam time at third-generation light sources.

Within this paper, we presented an approach to collect, process and analyze single-crystal data sets as used at the Extreme Conditions beamline (ECB P02.2) at PETRA III, DESY, Hamburg, Germany. This includes the introduction of a new data format called Esperanto that is supported by the commercial software package *CrysAlis*^{Pro} and that provides a vehicle to transform the most common area detector data formats employed at high-pressure beamlines using appro-priate translator software. Such a conversion tool has been developed and currently allows the conversion of tiff data collected by, for example, a Perkin Elmer detector into Esperanto format as well as modifying the header of data collected with MAR345/555 to provide more convenient interfacing with *CrysAlis*^{Pro} software. The approach was tested by collecting single-crystal diffraction data on boron-bearing mullite in the DAC at pressures up to 25 GPa. Details pertaining to the data collections and refinements of B-mullite at 19.4 GPa were presented.

APPENDIX A
CrysAlis^{Pro} Esperanto format specification

The file format has the extension *.esperanto or *.esper. It consists of an ASCII header followed by an uncompressed binary stream of long (4-byte) 'little' endian type.

The format supports image sizes ranging from 256×256 to 4096×4096 pixels with image dimensions in x and y being a multiple of four. Hence, for example, an image extent of 257 in a single dimension is not supported and has to be padded to 260 or cut to 256. The aspect ratio of the image pixel counts in x and y is free and the images have to be corrected to spatial distortions (two-dimensional unwarped) if used as input for *CrysAlis*^{Pro}.

All header lines have to be present in the data file. Moreover, the pixel size must be given and has to be square (even though the header entry for this purpose might suggest otherwise).

All values of a specific header line have to be present as integer or float; the hex notation is used as an indicator for non-valid or unknown values (*e.g.* 'ABSTORUN labstorunscale' would read like 'ABSTORUN 0x0' with labstorunscale treated as unknown).

In the following, (M) denotes a must value, *i.e.* it can never be hex. Optional values are indicated by (O). A string value is given in double quotes as text qualifier. If a string is non-valid/unknown it is marked by 'notvalidstring'.

A 'Hungarian pre-fix nomenclature' is used to label the bit depth internally used in *CrysAlis*^{Pro}: b, byte (1 byte); i, short (2 bytes); l, long (4 bytes); d, double (8 bytes). The *CrysAlis*^{Pro} header interpreter loads all numbers as doubles and then formats them to the given format; for example, the x image dimension 'lnx' will be read as a double and then casted into a long value as indicated by the prefix. Multiple spaces between numbers and/or strings are allowed; tabs are not allowed. Values, which are coded as 'Agilent internal' have no meaning for non-Agilent image formats and should be set to 0 or 0x0. These values helped during the format development to cross check Agilent image format with the exported Esperanto format. Esperanto format users should take care about (M) denoted values.

In the following, the header description for format version 1.1 is given.

All header lines have a fixed length of 256 bytes with 254 characters for content and the last two bytes for padding ('0d 0a' in hex). The first line gives the Esperanto format version and the total header length:

```
ESPERANTO FORMAT 1.1 CONSISTING OF 25 LINES OF 256 BYTES EACH
```

From the second line, keywords are used to provide information on the image dimensions and settings of the experiment such as geometry or wavelength. Every header line begins with a keyword followed by a number of parameters as given in Table 2. The parameters are separated by white spaces.

APPENDIX *B*
Example header of the Esperanto file format used at ECB P02.2, PETRA III

An example of a resulting header obtained from the conversion tool used at the ECB/P02.2 is given below. For simplicity, we have cut down the header to its bare minimum. Each row

in the original header has a fixed length of 256 characters with the last two characters being '0d 0a' (hex) resp. '13 10' (decimal):

```
ESPARANTO FORMAT 1.10000 CONSISTING OF 20 LINES OF 256 BYTES EACH
IMAGE 2048 2048 1 1 "4BYTE_LONG"
SPECIAL_CCD_1 0.00000000 0 0 0.00000000 0.00000000 0.00000000
SPECIAL_CCD_2 0 0 0 0 0
SPECIAL_CCD_3 0 0 0 0 0
SPECIAL_CCD_4 0 0 0 0 0 0 0
SPECIAL_CCD_5 0.00000000 0.00000000 0.00000000 0.00000000
TIME 1.0000000 0.00000000 0.00000000
MONITOR 0 0 0 0
PIXELSIZE 0.20000000 0.20000000
TIMESTAMP "Mon Jan 21 23 : 15 : 24 2013"
GRIDPATTERN "notvalidstring"
STARTANGLESINDEG 0.00000000 0.00000000 0.00000000 40.000000
ENDANGLESINDEG 0.00000000 0.00000000 0.00000000 44.000000
GONIOMODEL_1 0.00000000 0.00000000 0.00000000 0.00000000
   0.00000000 1078.0000 905.00000 0.00000000 0.00000000 0.00000000
GONIOMODEL_2 0.00000000 0.00000000 0.00000000 0.00000000
WAVELENGTH 0.28988 0.28988 0.28988 0.28988
MONOCHROMATOR 0.9900000 SYNCHROTRON
ABSTORUN 0
HISTORY "Esperanto generated by program conv_for_crysalis v. 0.3
 at ECB P02.2, PETRA III"
```

The settings[2] given in the above example (and the program default settings) have been chosen with respect to the standard setting at beamline P02.2 and the standard detector, XRD1621 from Perkin Elmer.

APPENDIX *C*
Further details on data processing and parameter setting for analysis

In order to prepare image data for further analysis with the software package *CrysAlis*^{Pro} from Agilent Technologies (Agilent, 2013), we developed a converter tool. Currently, it can convert image formats of the MAR345 (compressed in all resolutions, *i.e.* 1500, 2300, 3450) as well as tiff images. Depending on the selected detector format, the tool will transfer/treat data in a different manner.

C1. MAR specific imagery treatment: image header modification

In this particular case, the MAR detector is not storing any additional angular parameters like χ or ω in the header of individual images, *i.e.* the in-house script is just triggering the image readout. For data reduction within *CrysAlis*^{Pro}, one has to modify this information in the image header since the program extracts relevant diffractometer properties from the file header and does not support full modification of relevant parameters inside the program itself.

[2] Please note that the number given in the line labeled MONOCHROMATOR in general cannot be 1, but rather, for example, 0.98 as the polarization factor of the optics (or 0.02 in case of $90°$ turned set-up).

Table 2
File header description for *CrysAlis*[Pro] Esperanto format [based on the help document of version 171.36.28 (Agilent, 2013)].

IMAGE lnx lny lbx lby spixelformat	
lnx (M)	Image dimension in x direction in pixel count
lny (M)	Image dimension in y direction in pixel count
lbx (M)	Binning of the image in x direction in pixel
lby (M)	Binning of the image in y direction in pixel
spixelformat (M)	Bit depth of the binary stream (currently allowed 4BYTE_LONG)

SPECIAL_CCD_1 delectronsperadu ldarkcorrectionswitch lfloodfieldcorrectionswitch/mode dsystemdcdb2gain ddarksignal dreadnoiserms	
delectronsperadu (O)	Conversion electrons/ADU in case of scaled images (CCS camera has 2.1, fip60 cameras 1.0, ApexII 10-15)
ldarkcorrectionswitch (O)	0,1 to indicate dark correction
lfloodfieldcorrectionswitch/mode (O)	Specifier for type of flood correction (Agilent internal, 0 can be used for all non-Agilent)
dsystemdcdb2gain (O)	System gain for DCDB2 ('double correlated divided by 2') mode. Note: historically, *CrysAlis*[Pro] correlated images and divided them by 2; such images have half of the camera gain. For example, Atlas has a camera gain of 180, but its dsystemdcdb2gain is 90. See also SPECIAL_CCD_5 dtrueimagegain
ddarksignal (O)	In ADUs
dreadnoiserms (O)	In ADUs

SPECIAL_CCD_2 ioverflowflag ioverflowafterremeasureflag inumofdarkcurrentimages inumofmultipleimages loverflowthreshold	
ioverflowflag (O)	Indicator for overflow occurrence in base exposure. Options are: 0: No; 1: Yes; 0x0: unused
ioverflowafterremeasureflag (O)	Indicator for overflow occurrence in fastest/highest filter remeasure. Options are: 0: No; 1: Yes
inumofdarkcurrentimages (O)	Number of dark current images taken
inumofmultipleimages (O)	The image is the result of an image pile-up. inumofmultipleimages gives the number of images added together
loverflowthreshold (O)	ADU level at which the image is considered an overflow in base exposure

SPECIAL_CCD_3 ldetector_descriptor lisskipcorrelation lremeasureturbomode bfsoftbinningflag bflownoisemodeflag	
ldetector_descriptor (O)	Description for type of detector (Agilent internal): 0 can be used for all non-Agilent, remaining entries are then ignored for processing
lisskipcorrelation (O)	Indicator for skipped image correlation. Options are: 0: No; 1: Yes; 0x0: unused
lremeasureturbomode (O)	Indicator for usage of 'remeasure turbo' (Agilent internal). 0 can be used for all non-Agilent
bfsoftbinningflag (O)	Indicator for soft binning. Options are: 0: No; 1: Yes; 0x0: unused
bflownoisemodeflag (O)	Indicator for usage of 'low noise mode' (Agilent internal). 0 can be used for all non-Agilent

SPECIAL_CCD_4 lremeasureinturbo_done lisoverflowthresholdchanged loverflowthresholdfromimage lisdarksignalchanged lisreadnoisermschanged lisdarkdone lisremeasurewithskipcorrelation lcorrelationshift	
lremeasureinturbo_done (O)	Indicator for usage of 'remeasure turbo' (Agilent internal). 0 can be used for all non-Agilent
lisoverflowthresholdchanged (O)	Indicator for changing overflow threshold. Options are: 0: No; 1: Yes; 0x0: unused
loverflowthresholdfromimage (O)	Indicator that overflow threshold is from image. Options are: 0: No; 1: Yes; 0x0: unused
lisdarksignalchanged (O)	Indicator for changing dark signal. Options are: 0: No; 1: Yes; 0x0: unused
lisreadnoisermschanged (O)	Indicator for changing read noise. Options are: 0: No; 1: Yes; 0x0: unused
lisdarkdone (O)	Indicator that a dark image was done. Options are: 0: No; 1: Yes; 0x0: unused
lisremeasurewithskipcorrelation (O)	Indicator that a remeasure procedure was done without correlation. Options are: 0: Yes; 1: No
lcorrelationshift (O)	Value for correlation shift operation (Agilent internal). 0 can be used for all non-Agilent

SPECIAL_CCD_5 dblessingrej ddarksignalfromimage dreadnoisermsfromimage dtrueimagegain	
dblessingrej (O)	Blessing reject parameter (Agilent internal). 0 can be used for all non-Agilent
ddarksignalfromimage (O)	Self-explaining (Agilent internal)
dreadnoisermsfromimage (O)	Self-explaining (Agilent internal)
dtrueimagegain (O)	Actual gain for the image (Agilent internal)

TIME dexposuretimeinsec doverflowtimeinsec doverflowfilter	
dexposuretimeinsec (M)	Base exposure time in seconds. For correlated frames the time of one frame
doverflowtimeinsec (O)	Time used to bring frame in range
doverflowfilter (O)	Overflow filter used. Options are: 0: No; 1: Yes

MONITOR lmon1 lmon2 lmon3 lmon4	
lmon1 (O)	Monitor signal channel 1
lmon2 (O)	Monitor signal channel 2
lmon3 (O)	Monitor signal channel 3
lmon4 (O)	Monitor signal channel 4

ABSTORUN labstorunscale	
labstorunscale (O)	Value for abstorun procedure (Agilent internal). 0 can be used for all non-Agilent

Table 2 (continued)

PIXELSIZE drealpixelsizex drealpixelsizey	
drealpixelsizex (M)	Pixel size along x direction in mm
drealpixelsizey (M)	Pixel size along y direction in mm Note: drealpixelsizex = drealpixelsizey is a requirement

TIMESTAMP timestampstring	
timestampstring (O)	A string containing a time stamp (not used by $CrysAlis^{Pro}$, but useful for documentation purpose)

GRIDPATTERN filename	
filename (O)	The Esperanto images have to be distortion free. The filename documents the grid name (Agilent internal)

STARTANGLESINDEG om th ka ph	
dom dth dka dph (M)	Goniometer angles ω, θ, κ and φ in degrees, see Paciorek $et\ al.$ (1999) for details

ENDANGLESINDEG om th ka ph	
dom dth dka dph (M)	Goniometer angles in degrees, see above

GONIOMODEL_1 dbeam2indeg dbeam3indeg detectorrotindeg_x detectorrotindeg_y detectorrotindeg_z dxorigininpix dyorigininpix dalphaindeg dbetaindeg ddistanceinmm	
dbeam2indeg (O)	See Paciorek $et\ al.$ (1999) for details
dbeam3indeg (O)	See Paciorek $et\ al.$ (1999) for details
detectorrotindeg_x (O)	See Paciorek $et\ al.$ (1999) for details
detectorrotindeg_y (O)	See Paciorek $et\ al.$ (1999) for details
detectorrotindeg_z (O)	See Paciorek $et\ al.$ (1999) for details
dxorigininpix (M)	Beam center in x direction given in pixel (counting from 0); see Paciorek $et\ al.$ (1999) for details
dyorigininpix (M)	Beam center in y direction given in pixel (counting from 0); see Paciorek $et\ al.$ (1999) for details
dalphaindeg (M)	See Paciorek $et\ al.$ (1999) for details
dbetaindeg (M)	See Paciorek $et\ al.$ (1999) for details
ddistanceinmm (M)	Sample to detector distance in millimeter (sample to detection surface, $e.g.$ in CCDs the scintillator); see Paciorek $et\ al.$ (1999) for details

GONIOMODEL_2 dzerocorrectionsoftindeg_om dzerocorrectionsoftindeg_th dzerocorrectionsoftindeg_ka dzerocorrectionsoftindeg_ph	
dzerocorrectionsoftindeg_om (O)	See Paciorek $et\ al.$ (1999) for details
dzerocorrectionsoftindeg_th (O)	See Paciorek $et\ al.$ (1999) for details
dzerocorrectionsoftindeg_ka (O)	See Paciorek $et\ al.$ (1999) for details
dzerocorrectionsoftindeg_ph (O)	See Paciorek $et\ al.$ (1999) for details

WAVELENGTH dalpha1 dalpha2 dalpha12 dbeta1	
dalpha1 (M)	Self-explaining (in Å)
dalpha2 (O)	Self-explaining (in Å)
dalpha12 (O)	Self-explaining (in Å)
dbeta1 (O)	Self-explaining (in Å) Note: for synchrotron radiation one can provide the same wavelength for all four entries. In case one provides a single value for dalpha1, the optional arguments have to be 0x0

MONOCHROMATOR (ddvalue–prepolfac) (orientation–type)	
(ddvalue–prepolfac) (O)	For 'E1E3PLANE', 'E1E2PLANE' ddvalue; for 'SYNCHROTRON' prepolfac
(orientation–type) (O)	Keywords: E1E2PLANE, E1E3PLANE, or SYNCHROTRON. Note: SYNCHROTRON also comprises mirrors

| HISTORY historystring	
historystring (O)	Some image processing history for documentation. Note: limited to single line

When preparing data obtained by the MAR detector with the new tool, the ASCII as well as the binary part of the file header content is manipulated and a new output file is created. The (compressed) data part (*i.e.* the image data itself) is just copied into the newly created output file.

Header options that can be modified for the preparation of MAR image files are defined as tool header options 'Parameters', 'startanglesindeg' and 'endanglesindeg' (see Fig. 5). Under the option 'Parameters', one can modify the wavelength in Å, the sample-to-detector distance (sam_det_dist) in mm, and the center coordinates center_x and center_y of the image pattern in pixels. In the current implementation of the tool, values for ω (OM), 2θ (TH) and χ (CH) are set to zero despite the option for defining numbers in the table of entries. Values for φ are derived with respect to the numbers given for start and $\delta\varphi$ in the top level of the tool (see Fig. 2) and are modified during conversion.

The binary part of the header (*i.e.* corresponding numbers for wavelength, distance and center coordinates located in the
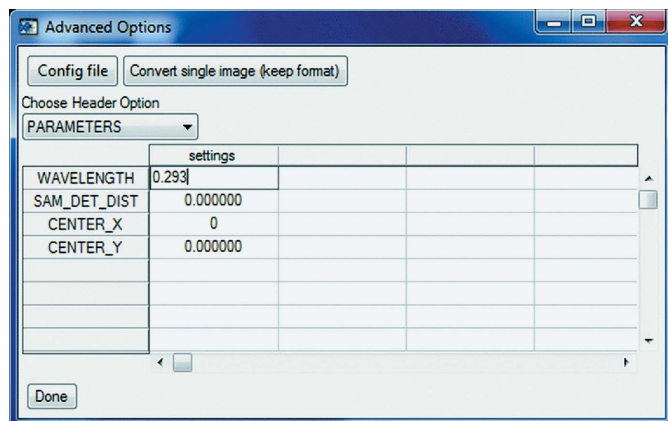
Figure 5
Sub-menu of the conversion tool. For MAR345/555 detectors (Mar-research GmbH), the header information can be modified according to the MAR345 format definition (Klein, 1997) which can be read by *CrysAlis*^{Pro} software.

first 16 words of 32-bit integers) is modified according to the MAR format definition (Klein, 1997).

C2. Perkin Elmer (or tiff) specific imagery treatment; conversion into Esperanto format from *CrysAlis*^{Pro}

The Perkin Elmer detector writes images in tiff format that is not supported by *CrysAlis*^{Pro}. Such data can be converted into the Agilent Technologies XRD Esperanto format, which was created to provide a means to interface unsupported image formats with *CrysAlis*^{Pro}. The Esperanto format in its current implementation (version 1.1) covers experiments conducted on four-circle diffractometers with area detectors as described by Paciorek *et al.* (1999). File extensions used for the format are *.esperanto or *.esper.

The format consists of an ASCII header providing format information (*e.g.* version number and binary type), parameters of the instrument (φ, χ, ω and 2θ) as well as information of the experiment itself (*e.g.* axis orientations, pixel sizes, wavelength in Å or scan angles). The following is the binary portion of the file containing the data of the image (stored as signed 4-byte long, little endian, uncompressed). Detailed specification of the format is given in Appendix *A*; header options provided by the tool are illustrated in Fig. 6.

In the transformation tool, the user can define the header so that the transformed images contain the relevant information to describe the scan made during the experiment. The default header settings and selections are currently preset to reflect measurements undertaken at beamline P02.2 at PETRA III. However, they can be adjusted to match the settings at other beamlines. An example of a resulting header is given in Appendix *B*.

Portions of this research were carried out at beamline P02.2 at the light source PETRA III at DESY, a member of the Helmholtz Association.
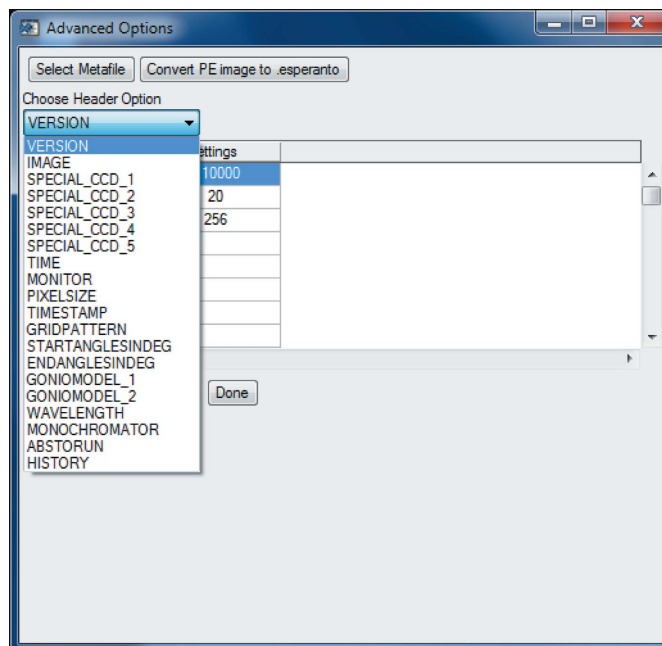
Figure 6
Sub-menu of the conversion tool. For Perkin Elmer detectors, header information as defined in the Esperanto format (see Appendix *A*) can be adjusted and image data can be converted into Esperanto format for further processing in *CrysAlis*^{Pro}.

References

Agilent (2013). *CrysAlis*^{Pro} Software System, version 1.171.36.28. Agilent Technologies UK Ltd, Oxford, UK.

Alfaro, M., Flemming, M., Grabitz, J., Kracht, T., Lewendel, B., Núñez, T., Reest, P., Rothkirch, A., Schlünzen, F. & Wintersberger, E. (2011). *Proceedings of the International Conference on Accelerator and Large Experimental Control Systems (ICALEPCS 2011)*, 10–14 October 2011, pp. 44–47.

Angel, R., Downs, R. & Finger, L. (2000). *Rev. Mineral. Geochem.* **41**, 559–596.

Angel, R. J., Bujak, M., Zhao, J., Gatta, G. D. & Jacobsen, S. D. (2007). *J. Appl. Cryst.* **40**, 26–32.

Boffa Ballaran, T., Kurnosov, A., Glazyrin, K., Frost, D., Merlini, M., Hanfland, M. & Caracas, R. (2012). *Earth Planet. Sci. Lett.* **333–334**, 181–190.

Chaimayo, W., Lundegaard, L., Loa, I., Stinton, G. W., Lennie, A. R. & McMahon, M. I. (2012). *High Press. Res.* **32**, 442–449.

Dera, P., Lavina, B., Borkowski, L. A., Prakapenka, V. B., Sutton, S. R., Rivers, M. L., Downs, R. T., Boctor, N. Z. & Prewitt, C. T. (2008). *Geophys. Res. Lett.* **35**, L10301.

Dera, P., Lavina, B., Meng, Y. & Prakapenka, V. (2011a). *J. Solid State Chem.* **184**, 3040–3049.

Dera, P., Lazarz, J., Prakapenka, V., Barkley, M. & Downs, R. (2011b). *Phys. Chem. Miner.* **38**, 517–529.

Dera, P., Prewitt, C. T. & Jacobsen, S. D. (2005). *J. Synchrotron Rad.* **12**, 547–548.

Dubrovinsky, L., Boffa-Ballaran, T., Glazyrin, K., Kurnosov, A., Frost, D., Merlini, M., Hanfland, M., Prakapenka, V., Schouwink, P., Pippinger, T. & Dubrovinskaia, N. (2010). *High Press. Res.* **30**, 620–633.

Gatta, G., Lotti, P., Merlini, M., Liermann, H.-P. & Fisch, M. (2013). *J. Am. Ceram. Soc.*, doi: 10.1111/jace.12411.

Gatta, G., Rotiroti, N., Fisch, M. & Armbruster, T. (2010). *Phys. Chem. Miner.* **37**, 227–236.

research papers

Guillaume, C., Gregoryanz, E., Degtyareva, O., McMahon, M. I., Hanfland, M., Evans, S., Guthrie, M., Sinogeikin, S. & Mao, H.-K. (2011). *Nat. Phys.* **7**, 211–214.

Hammersley, A., Svensson, S., Hanfland, M., Fitch, A. & Häusermann, D. (1996). *High Press. Res.* **14**, 235–248.

Jacobsen, S., Holl, C., Adams, K., Fischer, R., Martin, E., Bina, C., Lin, J., Prakapenka, V., Kubo, A. & Dera, P. (2008). *Am. Mineral.* **93**, 1823–1828.

Jennings, G. (1997). *QXRD: Readout Software for Flat Panel X-ray Detectors.* Structural Science Group, Advanced Photon Source, Argonne National Laboratory, Argonne, IL 60439, USA. [http://sourceforge.net/projects/qxrd/ (last accessed: 27 August 2012).]

Kantor, A., Kantor, I., Merlini, M., Glazyrin, K., Prescher, C., Hanfland, M. & Dubrovinsky, L. (2012). *Am. Mineral.* **97**, 1764–1770.

Klein, C. (1997). *mar345 formats*, http://www.marresearch.com/man/mar345_formats.htm (last accessed: 16 July 2013).

Klotz, S., Chervin, J.-C., Munsch, P. & Le Marchand, G. (2009). *J. Phys. D*, **42**, 075413.

Lavina, B., Dera, P., Downs, R., Tschauner, O., Yang, W., Shebanova, O. & Shen, G. (2010a). *High Press. Res.* **30**, 224–229.

Lavina, B., Dera, P., Downs, R., Yang, W., Sinogeikin, S., Meng, Y., Shen, G. & Schiferl, D. (2010b). *Phys. Rev. B*, **82**, 064110.

Lundegaard, L., Gregoryanz, E., McMahon, M. I., Guillaume, C., Loa, I. & Nelmes, R. (2009). *Phys. Rev. B*, **79**, 064105.

McMahon, M., Degtyareva, O., Hejny, C. & Nelmes, R. (2003). *High Press. Res.* **23**, 289–299.

McMahon, M., Degtyareva, O., Nelmes, R., van Smaalen, S. & Palatinus, L. (2007a). *Phys. Rev. B*, **75**, 184114.

McMahon, M., Gregoryanz, E., Lundegaard, L., Loa, I., Guillaume, C., Nelmes, R., Kleppe, A., Amboage, M., Wilhelm, H. & Jephcoat, A. (2007b). *Proc. Nat. Acad. Sci. USA*, **104**, 17297–17299.

Mao, H., Xu, J. & Bell, P. (1986). *J. Geophys. Res.* **91**, 4673–4676.

Marques, M., McMahon, M., Gregoryanz, E., Hanfland, M., Guillaume, C., Pickard, C., Ackland, G. & Nelmes, R. (2011). *Phys. Rev. Lett.* **106**, 095502.

Maynard-Casely, H., Bull, C., Guthrie, M., Loa, I., McMahon, M., Gregoryanz, E., Nelmes, R. & Loveday, J. (2010). *J. Chem. Phys.* **133**, 064504.

Merlini, M., Crichton, W. A., Hanfland, M., Gemmi, M., Müller, H., Kupenko, I. & Dubrovinsky, L. (2012a). *Proc. Nat. Acad. Sci. USA*, **109**, 13509–13514.

Merlini, M., Hanfland, M. & Crichton, W. (2012b). *Earth Planet. Sci. Lett.* **333–334**, 265–271.

Paciorek, W. A., Meyer, M. & Chapuis, G. (1999). *Acta Cryst.* A**55**, 543–557.

Petricek, V., Dusek, M. & Palatinus, L. (2006). *Jana2006. The Crystallographic Computing System.* Institute of Physics, Praha, Czech Republic.

Plonka, A. M., Dera, P., Irmen, P., Rivers, M. L., Ehm, L. & Parise, J. B. (2012). *Geophys. Res. Lett.* **39**, L24307.

Sokolova, Y., Azizov, A., Simonov, M. & Leonyuk, N. I. & Belov, N. (1978). *Dok. Akad. Nauk. SSSR*, **243**, 655–658.

Wong-Ng, W., Siegrist, T., DeTitta, G. T., Finger, L. W., Evans, H. T. Jr, Gabe, E. J., Enright, G. D., Armstrong, J. T., Levenson, M., Cook, L. P. & Hubbard, C. R. (2001). *J. Res. Natl Inst. Stand. Technol.* **106**, 1071–1094.

Zhang, J., Dera, P. & Bass, J. (2012). *Am. Mineral.* **97**, 1070–1074.